LASER INTERFEROMETER GRAVITATIONAL WAVE OBSERVATORY
- LIGO -
CALIFORNIA INSTITUTE OF TECHNOLOGY
MASSACHUSETTS INSTITUTE OF TECHNOLOGY

Technical Note	**LIGO-T1700275-v1**	2017/10/01

Characterizing Bulk Scatter in Crystalline Silicon

Amani Garvin —— Mentor Andrew Wade & Rana Adhikari

Distribution of this document:
LIGO Scientific Collaboration

California Institute of Technology
LIGO Project, MS 18-34
Pasadena, CA 91125
Phone (626) 395-2129
Fax (626) 304-9834
E-mail: info@ligo.caltech.edu

Massachusetts Institute of Technology
LIGO Project, Room NW17-161
Cambridge, MA 02139
Phone (617) 253-4824
Fax (617) 253-7014
E-mail: info@ligo.mit.edu

LIGO Hanford Observatory
Route 10, Mile Marker 2
Richland, WA 99352
Phone (509) 372-8106
Fax (509) 372-8137
E-mail: info@ligo.caltech.edu

LIGO Livingston Observatory
19100 LIGO Lane
Livingston, LA 70754
Phone (225) 686-3100
Fax (225) 686-7189
E-mail: info@ligo.caltech.edu

http://www.ligo.caltech.edu/

1 Introduction

The LIGO Voyager update is especially concerned with the material of the detectors optics. Current detectors use fused silica for the test mass mirrors; however, silica is not ideal for use in Voyager due to its thermal and mechanical properties at 123K. Silicon, however, works beautifully at 123K with low mechanical and thermal losses. Whats more important is that silicon mirrors can be made extremely pure at large volumes. However, there are still some expected defects in the silicon crystal. This project is focused on measuring the scatter as a diagnostic tool to measure the defect concentration in Michael Czochralski Magnetic Silicon. Beyond just using the scatter to understand the defect population in the Silicon, understanding the scatter by itself is important. Scatter from the mirrors can add phase noise, contribute to cavity loss, and disrupt squeeze states. In order to analyze scatter from silicon at 1550nm, a scatterometer was built to measure the scattered light as a function of angle. In order to characterize the defects that cause the scatter, these measurements are then compared to Mie scatter simulations of different expected populations of defects.

2 Michael Czochralski Silicon

Michael Czochralski magnetic field grown Silicon can be made with a low impurity density, with low absorption (5 ppm/cm), and at large disk diameters. The sample used in this experiment is a rectangle of magnetic field-grown Michael Czochralski Silicon with dimensions of 10x60x96 mm. The two 10x96 mm sides have a high quality parallel polish which were used previously for absorption measurements. One of the two 60x96mm sides has a moderate polish from which we will measure the scatter. In order to maximize the area through which the scatter is observed, the laser will transmit through the two 10x96 mm sides, and the scatter field will be recorded from the 60x96mm side. We expect to see a scatter field that correlates to Mie scattering from a population of void defects and oxygen precipitates in the Silicon.

The dominant defects in MC Silicon are void defects, that have an outer SiO2 layer. These voids are usually octahedral in shape, with sizes ranging from 70-200nm, with a layer of oxide around 5nm thick[1]. We can also expect to see some oxygen precipitates, which travel from the Quarts crucible that the crystal is grown from. However, due to the way that these crystals are made we expect more voids than oxygen scatterers.

Figure 1: Void Defect In Silicon

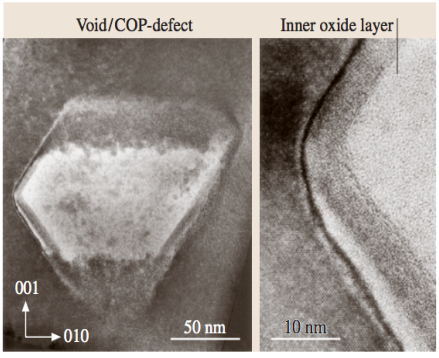

Since the defect population is related to the way the crystal is grown, it is important to review it. The crystal is grown using the Czochralski process. During this process, a mono-crystalline silicon seed crystal is immersed

[1] Defects in Monocrystalline Silicon, Ammon, Wilfried

into a vat of melted silicon. It is then pulled slowly out of
the mixture (a few cm/hour), and its pull speed determines the crystals diameter. During the growth of the crystal, the crystal as well as the crucible that holds the mixture, rotates. The Magnetic MC process adds a magnetic field to modify limit oxygen transport in the mixture[2].

3 Set Up of the Scatterometer

The scatterometer consists of an InGaAs camera which pivots around the Silicon sample, while the 1550nm laser goes through the samples side. The set up is shown below:

Figure 2: Scatterometer Set Up

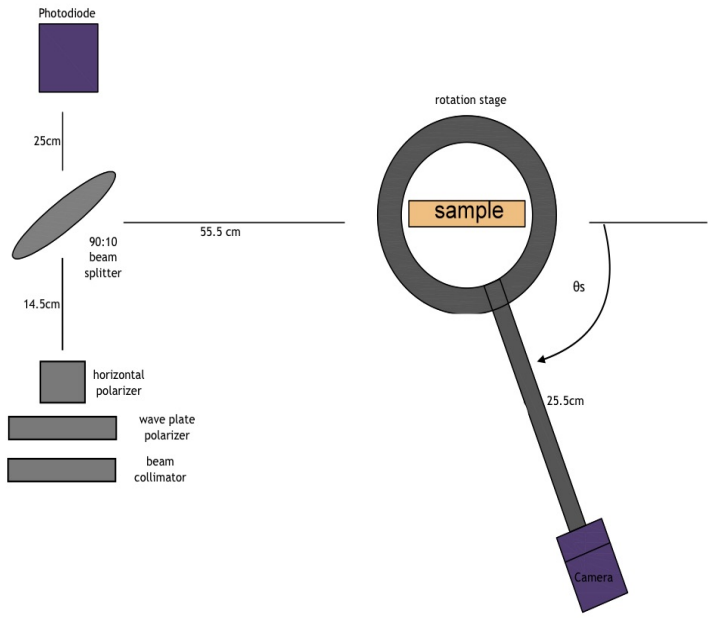

In the set up the 1550nm laser beam is collimated, and horizontally polarized (the wave plate polarizer also gives more control over the polarization of the laser beam). It is then split, so that

[2]http://www.microchemicals.com/products/wafers/silicon_ingot_production.html

1/10 of the beam's power can be measured, while the rest of the beam is sent through the Silicon.

The camera used in this experiment is a Wimby InGaAs camera, with an AR coated lens system. The camera has a spectral response from .9-1.7 μm, peak exposure time at 200ms, and resolution of 25 μm^2/pixel.

Figure 3: Wimby InGaAs Camera

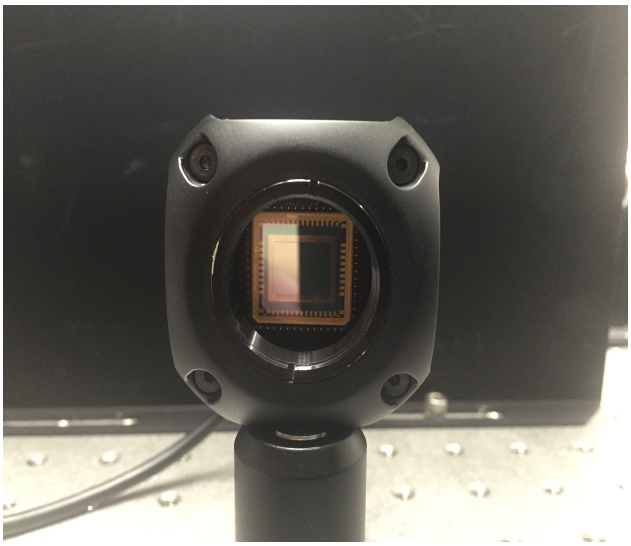

Figure 4: Camera On Rotation Stage

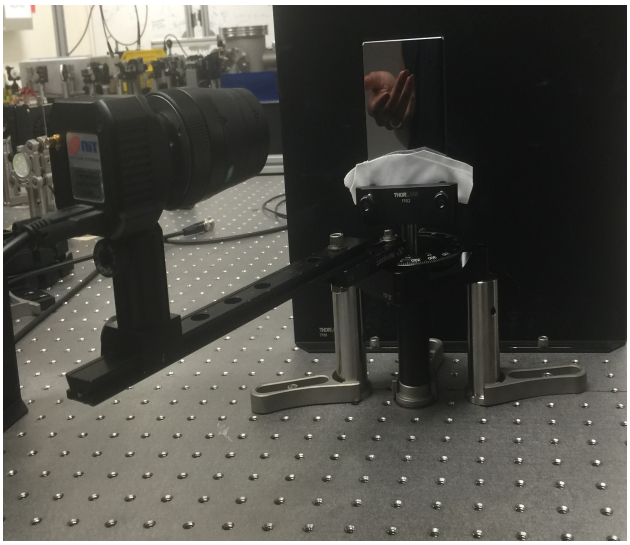

This makes it ideal for use at 1550nm, but not for 2000nm. This also means that for scatterers on orders of nanometers, our camera will not be able to resolve.

In order to measure the scattered field as a function of angle, the camera is placed on a rotation stage with a removable center. The silicon sample is then placed in the center of the rotation stage, so that the camera moves with respect to the sample at an angle.

4 Calibration

In order to calibrate the set up, both the photo diode and the camera had to be calibrated. For the photo diode, this was done by measuring the laser power with a power meter, and then reading the laser power out of the photo-diode with an oscilloscope. The power meter had a max power reading at 1.70mW. At gain 0, the photo-diode read a voltage of 2.60V. According to the photo-diode spec sheet, a gain of 0 corresponds to $1.5*10^5$ V/W. This gave a near one to one reading between the photo-diode and the power meter.

The next step was calibrating the camera. This was done by measuring a known scatter distribution, and comparing the cameras values to those values. The scatter function to be measured is Lambertian scatter, which can be seen by measuring light reflected off of white paper. This has a known BRDF (Bidirectional Scatter Distribution Function). The BRDF is defined as the quantity of reflected-light measured from a small surface element L_0 per quantity of incident light E_i:

$$BRDF = L_0/E_i \tag{1}$$

The total amount of incoming light arriving through the region is $L_i * dw$. In order to determine the amount of light with respect to the surface element, the incoming light must be projected onto the element by modulating it by $cos(\theta)$. This gives us the total amount of incoming light E_i:

$$E_i = L_i cos(\theta) * dwi \tag{2}$$

Which we can substitute into our initial expression of the BRDF:

$$BRDF = L_0/L_i cos(\theta) dwi \tag{3}$$

A Lambertian surface reflects light equally in all directions. And its BRDF is simply:

$$BRDF_{Lamb} = \rho/\pi \tag{4}$$

Where *rho* is its reflectivity, and can be assumed to be 1 for a white surface.

In order to calculate a calibration function, we must first normalize the camera's pixel counts by the exposure time and incindent power:

$$ARB_{camera} = \sum_k V_k/T_{exp}P_i \tag{5}$$

We can then calculate the calibration constant by taking the ration between the BRDF and the ARB:

$$F_c = BRDF/ARB_{camera} \tag{6}$$

This allows us to easily recover the BRDF from pixel counts recorded by the camera using the calibration constant:

$$BRDF = ARB_{camera} * F_c \tag{7}$$

This calibration was done using the setup constructed above, and replacing the sample with a white piece of paper. Following the procedure above resulted in a calibration constant of:

$$F_c = 3.73 * 10^{-12} Watt * sec * counts^{-1} * str^{-1} \tag{8}$$

Figure 5: Calibration With Lambertian Scatter

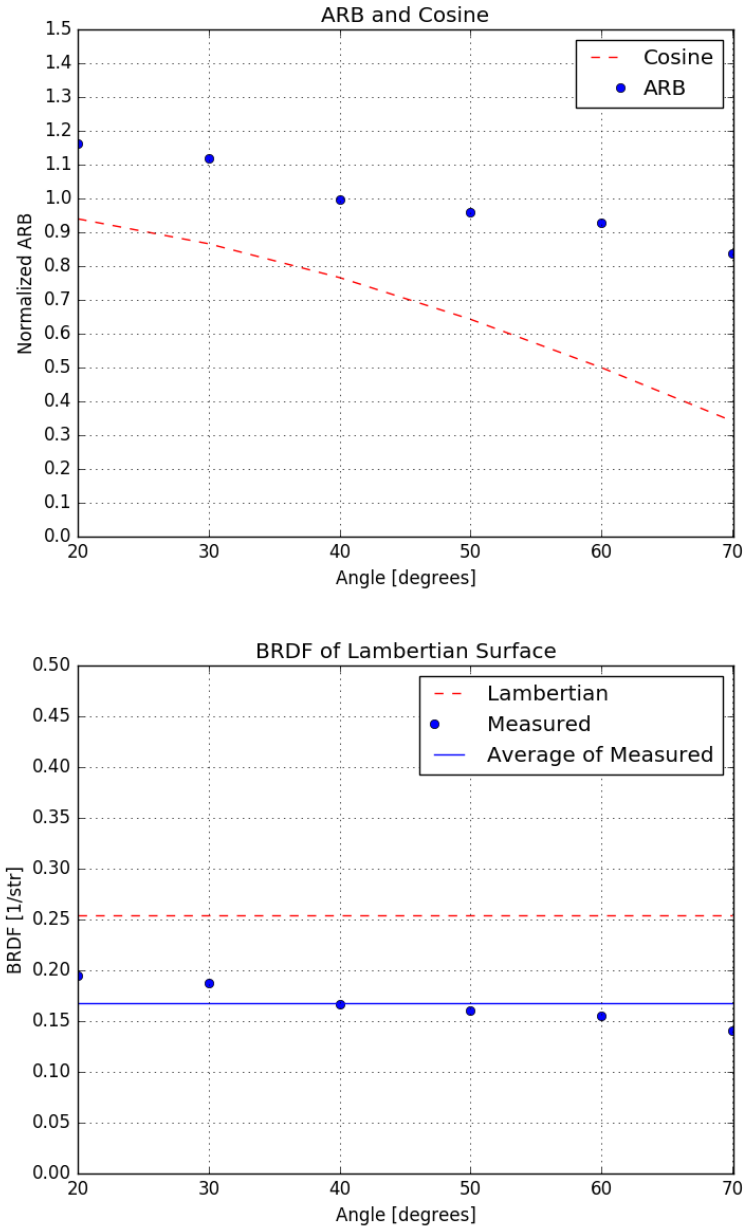

In the two images above, we have the normalized ARB of the camera plotted against the cosine function, and the BRDF of the sample plotted against an ideal Lambertian BRDF. From the first graph, we see that the ARB falls off loosely with cosine theta as expected. From the second graph we can see that there is a small constant offset between the measured BRDF and the ideal Lambertian BRDF. This is due to the assumption that the reflectivity of white paper is 1. However, typical reflectivity constants of white paper are closer to .8. We can recalculate our calibration constant, using a recorded value of paper reflectivity: .8.

$$F_c = 2.99 * 10^{-12} Watt * sec * counts^{-1} * str^{-1} \tag{9}$$

5 Image Processing

In order to view the laser going through the silicon, image processing tools were developed. Images are stored as 16-bit tiff files, these ensure that the data is uncompressed and covers the highest range possible. In order to get rid of hot pixels and any background signal, each image is background subtracted. This means that each view of the laser through the silicon sample is constructed by summing 100 images from that perspective. .

Figure 6: Sum of 100 images of the Silicon with the laser on

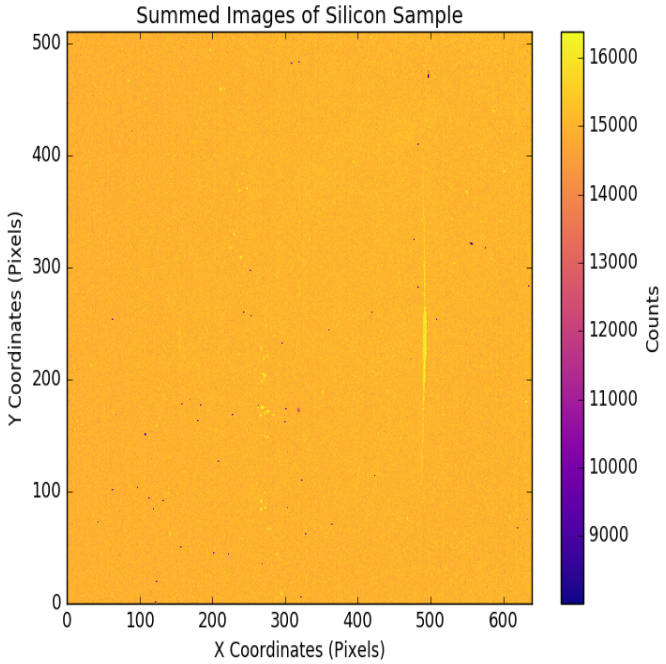

Then the laser is turned off and 100 images from that same perspective but with the laser off are summed. The summed dark image is then subtracted from the sum light image. This background subtraction accounts for hot pixels, and any environmental noise. The processing also accounts for over-subtraction, if any pixel was over-subtracted its value was set to zero

Figure 7: Background subtracted image of the silicon with the laser going through it

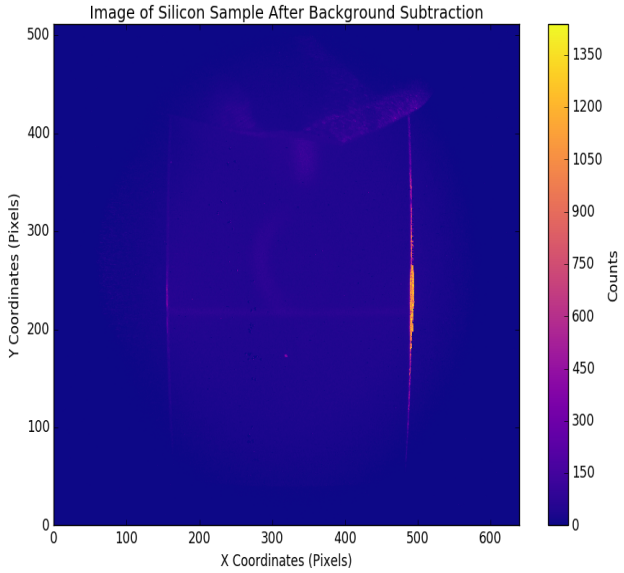

Once a background subtracted image is generated, we still can't see clearly the beam through the Silicon. It's obvious, by the bright spots on the sides, that the beam is going in and out of the Silicon. However, inside of the Silicon, the scattered light from the beam has a much lower signal than its surroundings. In order to tease out that signal, we look at the count distribution inside of the Silicon. This is done by first plotting the sum of pixel counts over the y-axis. This tells exactly where the beam is on the y-axis.

Figure 8: Sum of Counts Over the Y-Axis of the Image

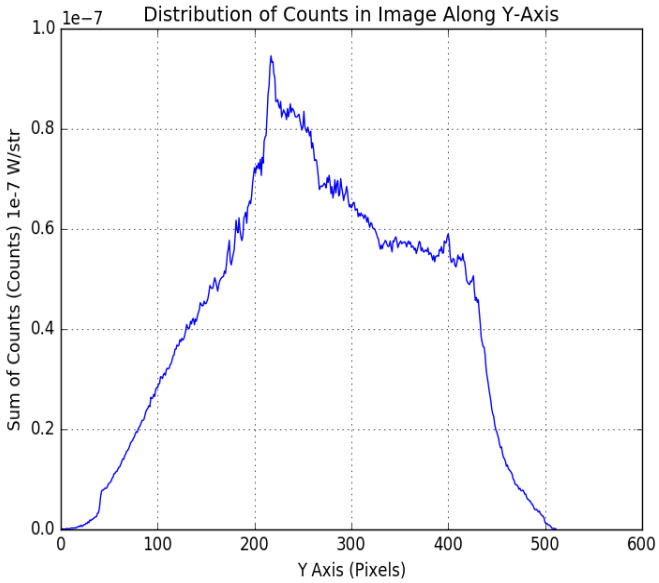

From looking at this image, we can see that there is a very sharp peak between 210 and 220 pixels, on the y-axis. We now sum the counts along the x-axis, that are between 210 and 220 pixels on the y-axis. This should give us an idea of the number of counts we get from the beam.

Figure 9: Sum of Counts Over the X-Axis, Between 210-220 Pixels on the Y-axis

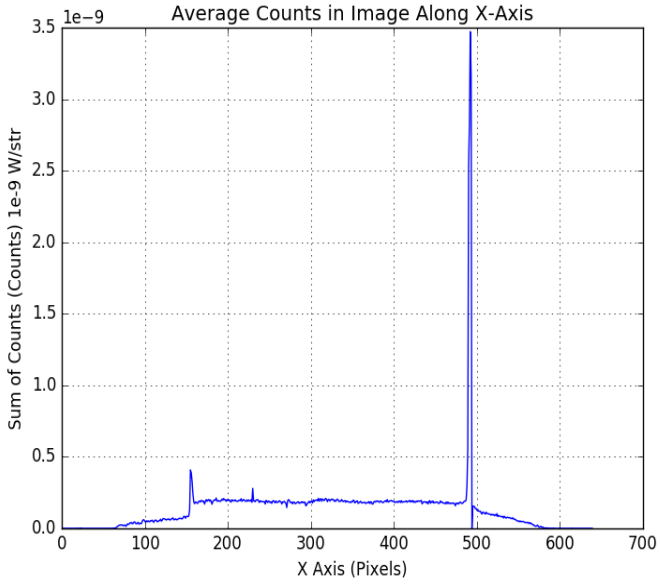

There are two sharp peaks at the edges, which come from the beam exiting the Silicon. Between those two peaks is a steady signal of about $.2039 * 10^{-9} W/str$. We can now rescale the image between zero and this signal.

Figure 10: Rescaled Image of the Laser Beam Through Silicon

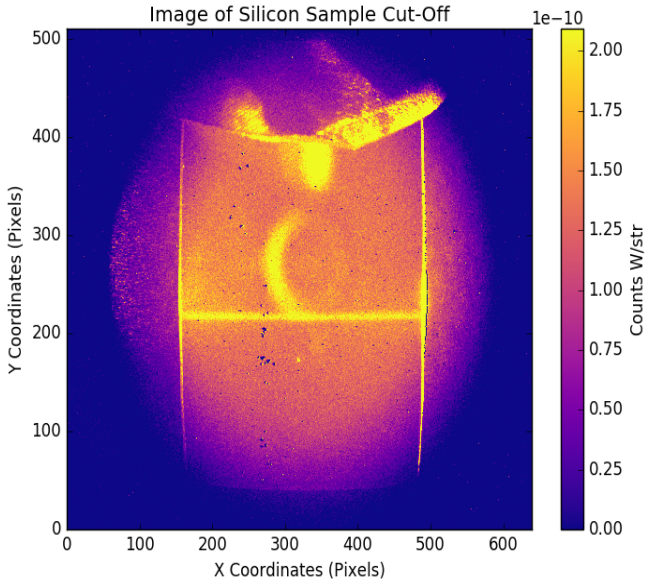

In this image, we clearly see the scattered beam through the Silicon, with a signal of $2*10^{-10}W/str$ and a background signal of $1.25*10^{-10}W/str$. The background could consist of other kinds of scatter or reflection inside of the Siicon. We can also see, above the flux limit we set, reflection from the lens, the strong bright spots from the laser exiting the silicon, and some reflection from the white cloth that is holding the sample in place on its stand. However we can now isolate the signal from its background.

6 Measuring The Scatter Field

The scattered field was first captured at 2 degree increments over a span of 100 degrees, for vertical polarization. It was then captured as a function of polarization angle. For each measurement, a rectangular region of interest capturing the laser beam is chosen. The total pixel count over this region is summed. For images as a function of scattering angle, the sums are normalized as a function of $cos(theta)$. These sums are then converted to a power scattered by using the calibration function, calculated earlier. It is then normalized by the incident laser power which was 28mW, as measured by the photo-diode.

Figure 11: BRDF of Silicon

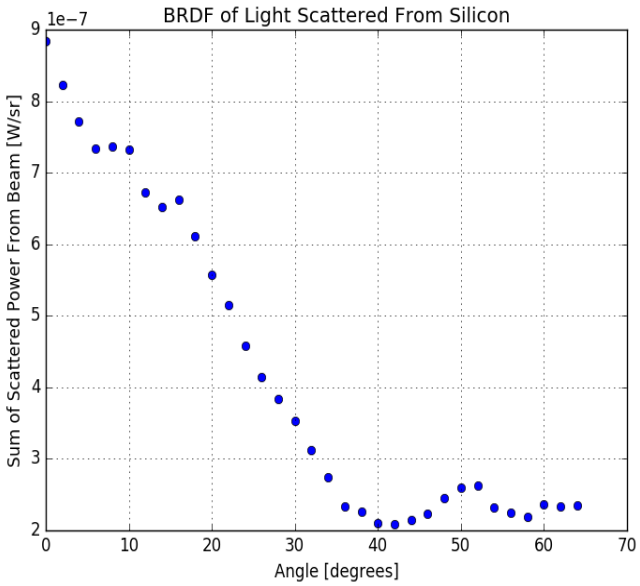

Figure 12: Ratio of Scatter Power To Incident Power As A Function of Polarization Angle

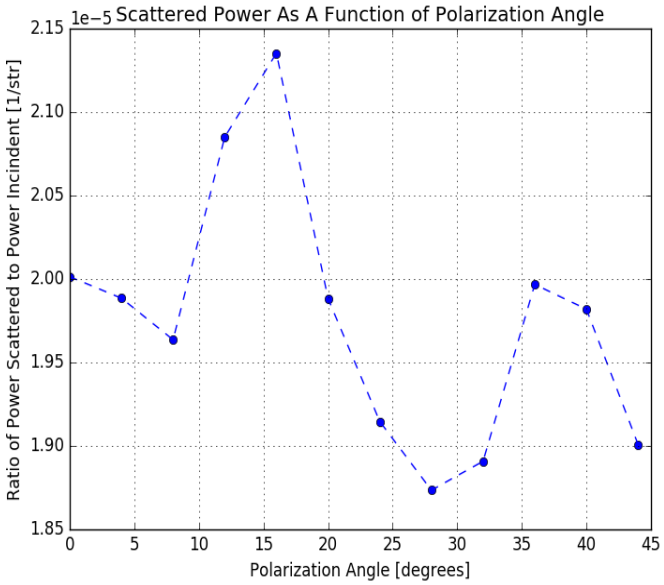

Looking at these graphs, we can see that the average scatter is around $1.95 * 10^{-5} str^{-1}$ and that there is no explicit polarization dependence. If Rayleigh scattering was dominant, there would be a $cos(\beta^2)$ dependency [3], where β is the polarization angle. This makes sense, since the populations that we expect has size on the order of 50-100nm, which is within an order of magnitude of the wavelength we are using. This means that we can expect Mie scattering dominating from our population of scatterers.

Using simulations of Mie scattering from single scatterers[4], we can estimate the dominant scattering population in the Silicon. The simulation provides exact solutions to light scattered by a homogeneous sphere of material, given wavelength, incident intensity, the refractive index of the material and the scatterer. Assuming that the refractive index of the Silicon sample is 3.673 at a wavelength of 1550nm, with an incident intensity of 356.5 W/m^2 [5], the simulations were run for a series of expected scatterers. The first population of scatterers, were oxygen from 50-200nm in size, with a refractive index of 1.000.

[3] Low scatter and ultra-low reflectivity measured in a fused silica window, Padilla et. al

[4] http://philiplaven.com/mieplot.htm

[5] 28mW over a beam with a 5mm width

Figure 13: Mie Scatter Simulation of Oxygen particles in Silicon for 1550nm

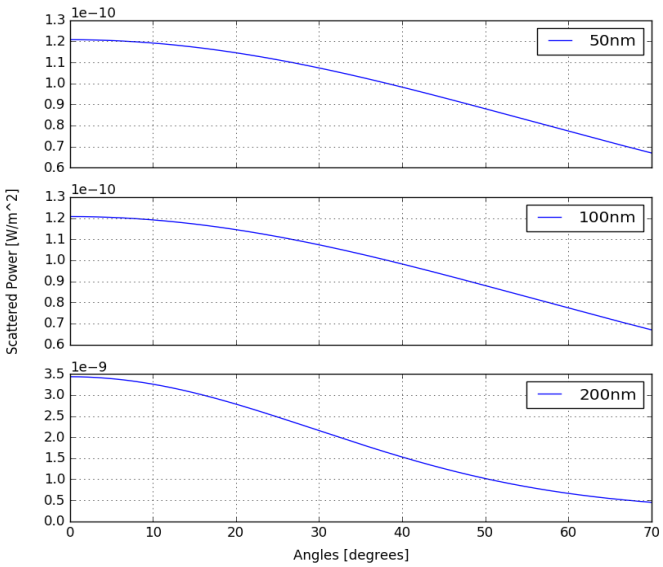

All of these curves decrease over scattering angle. There is also some leveling off from 60-70 degrees. The intensity for 50-100nm oxygen particles is on the order of 10^{-10} W/m^2, which is on the order of image's signal. We can also look at Silicon , with a refractive index of 1.444, which is the material that is expected in the voids.

Figure 14: Mie Scatter Simulation of Silicon Dioxide Particles in Silicon from 1550nm

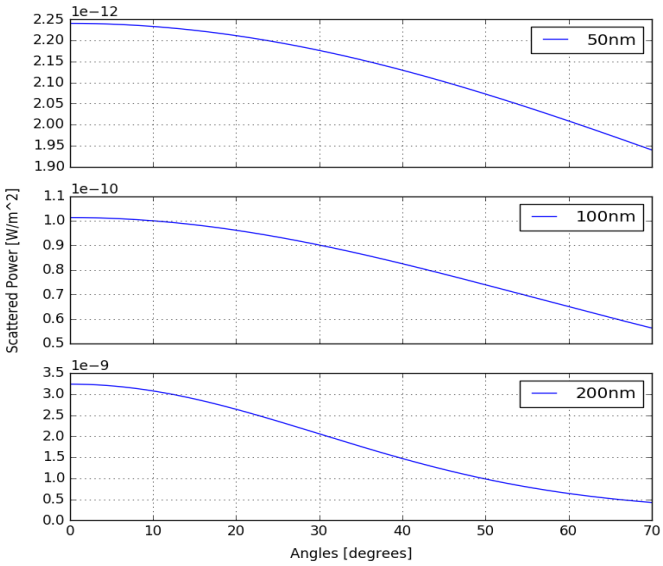

These curves also decrease over scattering angle. However, the intensity varies greatly, for 50nm the scatter is on the order of 10^{-12}, for 100nm it is on the order of 10^{-10}, and for 200nm, it is on

the order of 10^{-9}. The most likely one that we would observe in our sample is 100nm of Silicon Dioxide. Since we expect that the voids have a layer of oxide around some oxygen particles, then a population of 100nm scatterers producing mie scattering is very likely. There could also be oxygen precipates causing this scatter, however without being able to fully resolve scatterers, they can't be distinguished from the void population

7 Conclusion

With a total integrated scatter of 10^{-6} sr^{-1}, the scatter from the Silicon is fairly low. By comparing the measured scattered field with simulations of mie scattering from individual particles, we were able to get order of magnitude estimates of the scatter population. Assuming that all of the scatter is coming from one source, it's likely that it is caused by voids in the Silicon lattice. There could also be a population of oxygen precipitates, coming from the crucible, that can't be distinguished from the void population. Future work can be done to distinguish individual scatter populations, with a camera with higher resolution.